

Velocity modeling and attribute analysis to understand the gas hydrates and free gas system in the Mannar Basin, India

C. K. Mishra^{a,b}, P. Dewangan^{a,b}, R. Mukhopadhyay^c, D. Banerjee^c

^a CSIR - National Institute of Oceanography, Dona Paula, Goa, 403004, India

^b Academy of Scientific and Innovative Research (AcSIR), Ghaziabad, 201002, India

^c Geological survey of India, Mangalore, Karnataka, 575 001, India

Abstract

The Mannar basin, located between India and Sri Lanka, is a passive margin rift basin, is poorly explored for hydrocarbon compared to other petroliferous basins in the Indian offshore. 2D multichannel seismic data was acquired onboard *R/V Samudra Ratnakar* for exploring gas hydrate deposits in this basin. The bottom-simulating reflectors (BSRs) are observed in the seismic section, indicating the possible gas hydrate deposit. Several pull-down structures are identified below the BSR, suggesting the presence of free gas-bearing sediments. We also observed some chimney-like features, which extend from the deeper horizon up to the seafloor. An automated version of migration velocity analysis was used to estimate P-wave velocities along selected seismic lines. High interval velocities (> 1.7 km/s) are observed above the BSR for ~100 ms TWT across the chimney locations, indicating the presence of gas hydrates for the first time in the Mannar basin. Low velocities are observed below the BSR, indicating a widespread region of free gas-bearing sediments. Seismic attributes (instantaneous amplitude and frequency) analysis are used to demarcate the extent of these regions. Chimneys are identified as vertical zones of reduced amplitude, while the gas-bearing sediments below the BSR show high amplitudes and low-frequency. A deeper horizon ~800 ms TWT shows signatures associated with deep-seated gas reservoir. We propose that chimneys and small sub-vertical fractures provide pathways for the migration of deep-seated gases to shallower regions. The hydrate deposits of Mannar basin are unique as the organic-rich sediments are not supplied through any major rivers rather they are derived from the high biomass due to unusual physiography of the Mannar basin.

Keywords: Migration velocity analysis, BSR, Gas hydrates, Instantaneous Amplitude, Instantaneous frequency, Deep-seated gas reservoir

1. Introduction

Gas hydrates are ice-like crystalline substance formed by combining water with light hydrocarbon gases at high pressures and low temperatures (Sloan and Koh, 2007). Gas hydrates are abundant in the deep-oceanic and permafrost regions (Kvenvolden, 1993), and methane (CH₄) is the most common gas trapped in hydrates. Methane hydrate occurs in various forms like nodules, massive, dispersed in pore spaces, veins/fracture/faults, and layered horizons (Pellenbarg et al., 2000; Rice, 2006; Sadeq et al., 2018). It is unstable at standard pressure and temperature conditions, and 1 m³ of methane hydrate upon dissociation yields about 164 m³ of methane and 0.87 m³ of freshwater (Kvenvolden, 1993; Sloan and Koh, 2007). Methane hydrate acts like a huge reservoir to store methane gas; therefore, it is often treated as a non-conventional energy resource (Boswell and Collett, 2011; Kvenvolden, 1998; Milkov and Sassen, 2003). Methane is also a potent greenhouse gas (Kvenvolden, 1988); therefore, it can act as a significant driver for climate change if it dissociates and escapes into the atmosphere. Methane hydrate provides stability to marine sediments in continental slope region and its dissociation may mobilize sediments triggering slope failure (Brown et al., 2006; Pecher et al., 2008; Ramprasad et al., 2011).

The presence of gas hydrate strongly affects the physical properties of marine sediments, and its occurrence can be inferred from 2D/3D multichannel seismic (MCS) data (Singh et al., 1993). An anomalous seismic reflector, known as bottom simulating reflector (BSR), usually marks gas hydrate deposits (Shipley et al., 1979; Singh et al., 1993; Pecher et al., 1996). BSR represents a phase boundary and occurs due to the impedance contrast between the overlying gas hydrate-bearing sediments and the underlying free gas-bearing sediments (Helgerud et al., 1999; Singh et al., 1993). BSR usually coincides with the base of gas hydrate stability zone (GHSZ), which depends on seafloor depth, sea bottom temperature, geothermal gradient, and phase curve of methane hydrate + seawater (Kvenvolden and McDonald, 1985; Shipley et al., 1979; Singh et al., 1993). However, drilling expeditions worldwide have shown that the BSR is not a reliable proxy for mapping gas hydrate deposits (Majumdar et al., 2016). A strong BSR can occur due to a small amount of free gas below the GHSZ without any significant amount of gas hydrates. An alternate proxy for mapping gas hydrate deposits is the velocity of marine sediments derived from seismic data. P-wave velocity increases for gas hydrate-bearing sediments and decreases for free gas-bearing sediments. The velocity maps have been used successfully to map gas hydrate deposits in several basins worldwide like the Krishna-Godavari basin (Mishra et al., 2020), Hikurangi basin (Crutchley et al., 2010), northern Cascadia continental slope (Yuan et al., 1996), NE south china sea margin (McDonnell et al., 2000), and Ulleung basin (Ryu et al., 2009).

The occurrence of gas hydrate and free gas-bearing sediments can also be inferred using numerous other seismic attributes like amplitude blanking (Chand and Minshull, 2003), amplitude variation with offset (AVO) (Ecker et al., 1998; Dewangan et al., 2007), pull-up/pull-down structures (Wu et al., 2005), low-frequency shadow (Castagna et al., 2003), and seismic chimneys (Crutchley et al., 2010). The preferential deposition of gas hydrates along high porosity layers in mixed sediments deposits reduces acoustic impedance, and the horizons become faint and indecipherable yielding amplitude blanking (Dillon and Paull, 1983; Lee and Dillon, 2001). Variation in amplitude with increasing offset can infer valuable information about free gas below the BSR and gas hydrate above it (Carcione and Tinivella, 2000; Castagna and Swan, 1997; Gullapalli et al., 2019; Sriram et al., 2013). The push-up and push-down phenomena refer to distortion of time migrated seismic images due to lateral variability in seismic velocity owing to the presence of gas hydrates or free gas (Berndt et al., 2003; Petersen et al., 2010; Westbrook et al., 2008). When seismic waves propagate through a viscoelastic medium, its high-frequency components are preferentially attenuated. As a result, low-frequency components become stronger than high-frequency components (Sheriff, 2002; Taner et al., 1979). This phenomenon causes low-frequency shadow and is successfully used for detecting hydrocarbons (Castagna et al., 2003). The shallow occurrence of gas hydrate is usually inferred from the presence of seismic chimney, a narrow pathway through which gases from deep-seated reservoir migrate to the seafloor. In exceptional cases, methane may escape the seafloor leading to the formation of cold seeps and pockmarks.

Gas hydrates are explored along the continental margins of India for more than twenty years. Some of the petroliferous basins like Krishna-Godavari (KG), Mahanadi, and Andaman are well explored, and drilling/coring activities carried out during NGHP-01 and NGHP-02 expeditions have confirmed gas hydrate deposits in these basins (Collett et al., 2014; Kumar et al., 2014, 2019). However, other promising petroliferous basins like the Mannar basin (Fig. 1) is relatively unexplored for gas hydrate deposits. A preliminary seismic signatures of gas hydrate/free gas system was reported from the Mannar basin (Dewangan et al., 2015), but a detailed study of gas hydrate deposit is lacking. Therefore, we attempt to establish gas hydrates deposits through seismic velocity and attributes. Further, we attempt to understand the gas hydrate system in the Mannar basin by integrating multidisciplinary information and comparing it with the established system in other basins like the KG basin, where structural features control the spatial distribution of gas hydrate deposits (Dewangan et al., 2010; Mishra et al., 2020).

In marine system, methane is produced by degradation of organic matter either through biogenic or thermogenic processes (Whiticar et al., 1986). In general, major river systems supply the required

organic matter for the formation of gas hydrate deposits. Examples from Indian continental margins include the Krishna and Godavari rivers providing organic-rich sediments to the KG basin (Mazumdar et al., 2007), Mahanadi river to the Mahanadi basin (Mazumdar et al., 2014; Kumar et al., 2014), Indus river to the Makran accretionary prism (Grevemeyer et al., 2000), and Irrawaddy/Salween/Sittang rivers to the Andaman forarc basin (Satyavani et al., 2008). Likewise, the organic matter for gas hydrate deposits in Hikurangi margin, New Zealand, is derived from Waipaoa River and its tributaries (Berryman et al., 2010), Hong/Pearl rivers deliver organic-rich sediments to the South China Sea (Trung, 2012), Mississippi River to the Gulf of Mexico (Goñi et al., 1997), the Danube/Dniepr/Dniestr rivers to the black sea (Popescu et al., 2007), Columbia River to the Cascadia margin (Hedges et al., 1999), Amazon River to the Amazon basin (Atlantic) (Maslin and Burns, 2000), etc. In this regard, gas hydrate deposits reported for the first time from the Mannar basin is unique as the basin lacks a major river system, and the primary source of organic-rich sediments is high marine biomass that gets deposited due to the unique physiography of Mannar basin (Madhupratap et al., 1992; Jagadeesan et al., 2013).

2. Geological settings of the Mannar basin

The Cauvery basin is a Mesozoic rift basin along the east coast of India located between 75°27' to 79°54' E longitudes and 10° 9' to 13°30' N latitudes. The Western Ghats bounds the basin on the west, the Eastern Ghats on the east and the south, and the ridges on the north, separating it from the Pennar basin (Narasimha et al., 1995; Rao et al., 2010). It extends over Tamil Nadu, Karnataka, Kerala, and Union Territory of Puducherry, covering a length of 560 km and a width of 245 km. The Cauvery basin initiated from Gondwanaland's break-up into India, Antarctic, and Australia continents during the Late Jurassic-Early Cretaceous (Rao et al., 2010; Talukdar, 1982). Numerous deep extensional faults developed in NE-SW direction during rifting, and active subsidence resulted in graben and horst structures (Bastia and Radhakrishna, 2012; Yanqun et al., 2017). Differential subsidence resulted in the formation of sub-basins within the Cauvery basin including the Gulf of Mannar. The Mannar sub-basin is situated in the south-east part of the Cauvery basin and is further divided into western and eastern segments by the NE-SW aligned Mandapam - Delft ridge (Rao et al., 2010). Curray (1984) opined that the first rifting between India, Sri Lanka, and Antarctica occurred through the Cauvery - Palk Strait - Gulf of Mannar zone; however, the rifting episode did not progress into the seafloor spreading stage.

3. Data and Methodology

Seismic data used in the present study were acquired by the geological survey of India (GSI) in collaboration with CSIR-National Institute of Oceanography (NIO), Goa onboard *RV Samudra Ratnakar* from 15th February to 20th March 2015. A dual airgun array with a total volume of 3000 cu. in. was used as a seismic energy source. A 3000 m long hydrophone array with 240 channels was used as a receiver. The shot interval was fixed at 25 m, and the receiver interval was 12.5 m with a near offset of 70 m and a far offset of 3070 m. The data were recorded for 8 s two way travel time (TWT) with a sampling interval of 1 ms. The CDP fold is 60, and the dominant frequency is ~50 Hz. In the present study, two inlines (EW03 and EW04) in the NNE-SSW direction and two cross lines (NS10 and NS11) in the WNW-ESE direction (Fig. 2) are used. The initial data processing was carried out using ProMax/SeisSpace® software package available at CSIR-NIO and GSI. The geometry was assigned to the raw data using the UKOOA P1/90 file. An F-K filter was applied to remove coherent noise generated from source and tail buoys and the ship propeller. A bandpass filter (10-20-125-250) was applied to suppress low- and high-frequency ambient noises in the data. The data are NMO corrected and stacked to obtain a seismic image. Finally, poststack migration is applied to position the reflectors correctly and the seismic section is used for interpretation. The automatic velocity analysis algorithm of Mishra et al. (2020) was used to generate high-spatial density interval velocities. In this method, the pre-processed seismic data is migrated over a range of constant velocities using Kirchhoff migration, and common image gathers (CIG) are generated for each velocity. The time-varying velocities that flatten the reflectors in CIG gathers are considered the correct migration velocities (Biondi and Symes, 2004; Sava and Biondi, 2004; Stork, 1992; Yilmaz, 2001). In order to measure the flatness of CIGs, semblance plots were generated as a function of migration velocities (1450-1850 km/s) and two-way travel times (TWT). Semblance is a normalized coherency measure varying between zero and unity (Taner and Koehler, 1969). Zero represents no coherence, while unity represents the highest coherence. Next, we follow Toldi (1989) for auto-picking of migration velocities through the semblance panel. The auto-picking is guided along user-defined horizons, which are well separated in time to minimize the error in interval velocities (Hajnal and Sereda, 1981). For every CIG, the initial velocities (velocity nodes) were picked for these horizons such that they represent maximum semblance corresponding to the horizon's time. Next, we generate a smooth 1-D velocity function in time that pass through all the velocity nodes, and compute the total semblance for this function. We estimate the final 1D-velocity model by maximizing the total semblance using the simplex method (Nelder and Mead, 1965). The estimated migration velocities are assumed to be RMS velocities and are converted to interval velocities using the Dix equation (Dix, 1955). The process is repeated for

each CIG to generate a 2D-velocity model, which is interpreted to identify anomalous high velocities (gas hydrate) and low velocities (free gas) zones.

4. Results

We identified BSR in patches along various seismic profiles based on its characteristic properties such as reverse polarity with respect to the seabed, mimicking to seafloor topography, and cross-cutting the background geological strata. Some examples of BSRs from lines EW-3, EW-4, NS-10, NS-11 along with multibeam bathymetry data are shown in Figure 3. The observed depth of the BSR is close to that computed from the thickness of gas hydrate stability zone (Rastogi et al., 1999). The seismic data and corresponding estimated interval velocities for selected profiles are shown in Figure 3.

4.1. Seismic velocities along north-south lines (NS10 and NS11)

Figure 3a shows the seismic image of line NS10 and its corresponding velocity model. A chimney-like structure is identified around CDP 2000, extending from 3.5 s TWT (two-way travel time) up to the seafloor. BSR coinciding with the base of GHSZ is observed in the vicinity of the chimney at 3.0 s TWT. The base of GHSZ is extended throughout the section and highlighted in Figure 3a. High amplitude reflectors are observed below the BSR from CDPs 1500 to 2300. Amplitude reduction is observed below these reflectors, indicating seismic attenuation due to the presence of free gas. Interval velocity profile shows low velocities below the BSR corresponding to the region of high amplitude reflectors and this low-velocity zone extends up to 500 ms TWT below the BSR. A ~100 ms TWT thick zone above the BSR shows high interval velocities (> 1.7 km/s) for these CDPs compared to the background velocity of ~1.65 km/s. Another anomalous patch of high velocities above the BSR and low velocities below the BSR is observed from CDPs 2700-3400.

Figure 3b shows the seismic image of line NS11 and its corresponding velocity model. A BSR is observed at the base of GHSZ (2.6 to 2.8 s TWT) near chimneys at CDPs 950 and 1550. Again, the base of GHSZ is extended throughout the section. A deeper horizon, below which seismic energy drops significantly, is observed at ~3.3 s TWT from CDPs 1600-4000 and will be referred to as gas horizon. We observed two chimney-like structures near CDPs 950 and 1550 in the seismic section, which are easily visualized in the seismic attributes. They rise vertically from the inferred gas horizon up to the seafloor. Moderately-high amplitude reflectors are observed from CDPs 700-1200 near the chimney at CDP 950, and they occur up to a depth of ~100 ms TWT below the BSR. In contrast, strong amplitude reflectors are observed over a wide range of CDPs from 1400-2400 near the chimney at CDP 1550, and they extend up to a depth of ~500 ms TWT below the BSR. A significant drop in amplitude is observed below these reflectors from CDPs 1600-2400. A zone of high interval velocities

(> 1.8 km/s) is observed up to ~150 ms TWT above the BSR from CDPs 850-1500 near the chimney at CDP 950. Likewise, slightly higher velocities (>1.65 km/s) are observed immediately above the BSR near the chimney at CDP 1550. A drastic reduction in velocity (< 1.5 km/s) is observed below the BSR in this zone. These low velocities extend immediately below the BSR to a depth of 500 ms TWT. Some additional patches showing a combination of high velocities/ low velocities above/below the BSR are also observed from CDPs 2400-3100.

4.2. Seismic velocities along east-west lines (EW03 and EW04)

Figure 3c shows the seismic section of line EW03 and its corresponding velocities. The deeper gas horizon is observed around 3.3 s TWT throughout the seismic line. Several patches of BSR are observed in the seismic data around 2.75 s TWT. High amplitude reflectors below the BSR display push-down structure, an artificial distortion in time-migrated seismic images due to an anomalous low velocities zone. Reflectors below this structure are attenuated and show lower frequencies. This phenomenon is more pronounced below the gas horizon. Seismic velocities in these attenuated zones (CDPs 1700-2000 and CDPs 2750-3200) are extremely low (< 1.4 km/s) as compared to the background velocity. Moderately-high velocities (>1.65 km/s) are observed in these zones above the BSR.

Figure 3d shows the seismic section of line EW04 and its corresponding velocities. The deeper gas horizon is observed below 3.0 s TWT throughout the seismic line. A prominent submarine channel is observed from CDPs 1200-2000, and patches of BSR are observed near 2.65 s TWT on either side of the channel. High amplitude reflectors are prominent on the left flank of channel immediately below the BSR. Reflectors below this zone show reduced amplitude and display lower frequency owing to seismic attenuation. On the channel's right flank, few high-amplitude reflectors are observed immediately below the BSR from CDPs 2300-3000. Seismic attenuation is not prominent below this region. Zones of low interval velocities (< 1.5 km/s) are observed along both the channel's flanks and extend from the BSR to the gas horizon. The background velocity of 1.65 km/s is observed away from low velocities zones. High velocities (> 1.65 km/s) are observed above BSR on the channel's left flank, while no significant anomaly is observed on the right flank.

4.3. Reliability of auto-picked velocities

We performed a quality check on the auto-picking algorithm to assess its reliability in estimating seismic velocity. The flatness of CIG is considered to be a measure for the accuracy of migration velocities (Biondi and Symes, 2004; Sava and Biondi, 2004) and is represented using semblance plots. In the present study, moderately-high semblance values (> 0.3) are considered suitable for velocity

model building; therefore, velocities associated with low semblance values (< 0.3) were discarded. A focused maximum on the semblance panel suggests good resolution in the estimated velocity.

The semblance plot for seismic line NS10 at CPD 1717 shows seafloor at 2.46 s TWT and BSR at 2.7 s TWT (Fig. 4a). Migration velocities start increasing from ~ 2.62 s TWT till the BSR and show a drop immediately below the BSR. A significant drop in interval velocity is observed below 3.25 s TWT, corresponding to the observed gas horizon (Fig. 3a). The semblance appears diffused, indicating poor resolution in velocity as the offset-to-depth ratio is smaller than unity. We have discarded the velocities for the gas horizon in the present study. The semblance plot for seismic section NS11 at CIG 1951 represents a high amplitude zone below the BSR (Fig. 4b). The seafloor is observed at 2.1 s TWT and BSR at 2.55 s TWT. An increase in velocities is observed from 2.4 to 2.55 s TWT above the BSR. A significant drop in velocity is observed below the BSR till 2.85 s TWT, corresponding to the high amplitude zone. A similar low-velocity trend is observed below 2.9 s TWT for the gas horizon; however, the auto-picking algorithm has not detected it because of low semblance values. Figure 4c shows a semblance plot of EW03 at CIGs 1776, representing high-amplitude low-velocity reflectors below the BSR. The seafloor is observed at ~ 2.32 s TWT and BSR at ~ 2.61 s TWT. A mild increase in velocity is observed from the seafloor up to 2.55 s, and a moderate increase is observed till the BSR. A significant decrease in velocity (< 1.5 km/s) is observed below the BSR till 2.9 s TWT. The velocity starts increasing again till 3.2 s TWT; a second low-velocity zone is observed for the deeper gas layer; however, the semblance is below the threshold value to be picked by the algorithm. Figure 4d shows a semblance plot for seismic line EW04 at CPDs 707, where a high reflective zone is observed below the BSR from CDPs 100-1250 (Fig. 3d). The seafloor is observed at 2.25 s TWT and BSR at 2.55 s TWT. No significant velocity anomaly is observed above the BSR; however, a minor decrease in velocity is observed below the BSR till 2.63 s TWT. A clear low-velocity trend is observed at the beginning of the gas horizon from 3.15 s to 3.3 s TWT, where faint reflectors are observed due to high seismic attenuation (Fig. 3d).

4.4. Seismic attributes analysis for selected seismic profiles

Seismic attributes like instantaneous amplitude and frequency can assist in gas hydrate exploration (Li et al., 2013; Riedel et al., 2010; Ojha and Sain, 2009). Instantaneous amplitude, a measure of reflectivity strength, can identify locales of high-reflective zones owing to gas hydrate or free gas-bearing sediments (Coren et al., 2001; Riedel et al., 2010,). It can also map low-reflective zones caused by the presence of gas hydrate (amplitude blanking) or due to the availability of free gas (high seismic attenuation). Instantaneous amplitude profile of line NS10 highlights seismic chimney as a blanking zone extending vertically upward from the top of the gas horizon up to the seafloor (Fig. 5a). High-

reflective zones are observed on either side of the chimney, indicating lateral transport of free gas. Low-amplitude reflectors are observed below the gas horizon. Two additional chimneys are observed in the seismic line NS11 at CDPs 950 and 1550 (Fig. 5b). They also extend vertically upward from the deeper gas horizon. Likewise, high reflective zones are observed on either side of both the chimneys and are very prominent from CDPs 1400 to 2000. Low-amplitude reflectors are observed just below this zone owing to strong seismic attenuation. Below the gas horizon, reflectors are observed from CDPs 500-1400; however, they become weak from 1400-2000 owing to high attenuation due to the presence of free gas below the BSR. Three prominent blanking zones representing chimneys are observed in line EW03 (Fig. 5c), which extend from the deeper gas horizon up to the BSR. Some chimneys may cut across BSR and reach close to the seafloor. In the region of patchy BSR (CDPs 1 to 3500), low reflectivity is observed below the gas horizon; however, relatively high amplitude reflectors are observed outside the BSR zone. Likewise, high amplitude reflectors are observed immediately below the BSRs (CDPs 1-1000 and 2000-3000) and low-amplitude reflectors (LAR) below them for seismic line EW04 (Fig. 5d).

Instantaneous frequency, defined as the temporal rate of change in instantaneous phase, is another seismic attribute useful in detecting low-frequency shadow in seismic data. The frequency profile for line NS10 (Fig. 6a) shows a continuous low-frequency zone below the observed gas horizon, which becomes more prominent after CDP 1800.

Low-frequency zones are also observed below the BSR corresponding to high amplitude reflectors (Fig. 5a and Fig. 6). A similar low-frequency zone is observed in the region of high amplitude reflectors for line NS11 (Fig. 6b); the region is also characterized by low velocities (Fig. 3b). Likewise, the regions displaying pull-down structures in line EW03 show lower frequency than that of surroundings (Fig. 6c). In the deeper section below the gas horizon, a continuous zone of low-frequency is observed from CDPs 100-2500. The frequency profile of the line EW04 also shows a continuous zone of very low-frequency below the gas horizon (Fig. 6d). In some patches, the low-frequency zones appear to rise vertically up and spread laterally in shallow subsurface between 2.6 and 3.1 s TWT.

5. Discussions

5.1. Geophysical evidence of gas hydrate deposits in the Mannar basin

In general, gas hydrate is inferred from the presence of BSR in seismic data (Shipley et al., 1979). BSRs are identified on several seismic profiles (Fig. 3), indicating the widespread occurrence of gas hydrate deposits in the Mannar basin. The seismic-derived interval velocity map is a reliable proxy for mapping gas hydrate and free gas-bearing sediments (Singh et al., 1993). Velocities are used to infer

gas hydrate and free gas deposits worldwide. For example, KG basin (Jaiswal et al., 2012b; Mishra et al., 2020), Hikurangi margin (Crutchley et al., 2016, 2010), offshore western Colombia (Minshull et al., 1994), offshore Peru (Pecher et al., 1996), northern Cascadia margin (Yuan et al., 1996), etc. The drilling/coring activity in the KG basin, eastern continental margin on India, shows that high-velocities (> 1.65 km/s) are linked to the presence of gas hydrate above BSR and low-velocities (< 1.5 km/s) corresponds to free gas below the BSR (Jaiswal et al., 2012a; Mishra et al., 2020). In the absence of drilling/coring data from the Mannar basin, we assume that the background sediment velocity in the Mannar basin is ~ 1.65 km/s, similar to that reported from the KG basin. High-velocities (>1.65 km/s) around chimney locations above the BSR likely represent the presence of gas hydrate deposits (Figs. 3a and 3b), whereas low-velocities (<1.5 km/s) beneath the BSR show the presence of gas-bearing sediments. Seismic attributes are also used to infer gas hydrate/free gas deposits (Li et al., 2013; Riedel et al., 2010). In the Mannar basin, the reflectors within the low-velocities zone show high amplitude in the seismic section (Figs. 3a,b), indicating free gas availability beneath the BSR. The reflectors beneath the gas layer show low amplitudes (Figs. 5c,d) and display lower frequencies (Figs 6c,d) due to high attenuation of the gas horizon. A push down structure is also identified within the seismic chimney (Figs. 3c and 3d), indicating anomalously low-velocity owing to the presence of free gas. All these observations collectively confirm the presence of free gas below the BSR, and seismic chimneys provide pathways for gas migration from deep-seated reservoir to the shallow subsurface. In the Mannar basin, we observed a deep-seated horizon with low-velocities which may be a potential gas reservoir.

5.2. Geological evidences of a cold-seep ecosystem in the Mannar basin

Analysis of seismic data suggests the presence of gas hydrate and free gas deposits in the Mannar basin. Fluid migrates from deep-seated gas reservoir to shallow subsurface through the fracture system, manifested in seismic data as chimneys. In exceptional cases, fluid/gas migrates up to the seafloor leading to a cold-seep ecosystem. One such pockmark was sampled onboard *RV Sindhu Sadhana* (Cruise No. SSD-070 from 12th - 23rd February 2020). Polychaete tubeworm associated with the chemosynthetic communities, authigenic carbonates with relict shells of *Calyptogena* sp., heterotrophs such as squat lobsters and gastropod are observed in the sediment samples acquired from pockmark region, confirming cold-seep ecosystem (Mazumdar et al., 2021). Sediment sampling from spade cores show the presence of polychaete tubeworm (Fig. 7a) and the gravity core revealed a shallow presence of fracture-filled methane hydrate (Figs. 7b,c).

5.3. Gas hydrate system in the Mannar basin

The spatial distribution of gas hydrates is observed to be structurally and stratigraphically controlled in different active and passive basins worldwide (Milkov and Sassen, 2002). In a structurally-controlled gas hydrate accumulation, fracture/fault systems provide an environment conducive to the migration of methane gas and the formation of methane hydrate. Examples of such deposits are reported from the KG basin (Mishra et al., 2020), northwest Gulf of Mexico (Milkov and Sassen, 2002, 2001; Sassen et al., 2001), Nankai trough (Yamamoto et al., 2014), Hikurangi margin (Crutchley et al., 2010), South China sea (Wu et al., 2005), mid- Norwegian continental margin (Bünz et al., 2003, Berndt, 2005). The region seismic lines in the Mannar Basin show no basin-scale tectonic fault systems; however, several small-scale local faults/fractures related to passive margin settings are observed. Integrated analysis of different seismic attributes (velocity, instantaneous amplitude, and frequency) and the identification of pockmarks and cold seeps show that chimneys' locations are favorable locales for hydrate formation in the Mannar basin. Seismic attributes show the presence of free gas below the BSR and within the chimneys.

We observed a deep-seated gas reservoir in this basin, and gases migrate from this horizon to the shallow subsurface through subsurface fractures or along some permeable horizons. These subsurface fractures are distributed randomly and may not be related to any tectonic activities. Such a fracture system typically occurs in a passive margin due to sediment compaction and fluid expulsion (Cartwright, 1994; Berndt et al., 2003). Fractures occur in a fine-grained sedimentary basin and provide pathways for fluid flow. Similar fault systems are observed in the mid-Norwegian passive continental margin and are associated with the gas hydrate deposits (Berndt et al., 2003). In the absence of any major faults or permeable horizon, gas movement is restricted and vast amounts of gas accumulate over time, yielding over-pressured sediments. Velocities increase with depth due to compaction and a sudden inversion indicates over-pressured sediments (Dutta et al., 2002). We propose that the observed low-velocity zone at greater depths show overpressured sediments in the Mannar basin. The over-pressured sediments may create faults/fractures near weak zones and facilitate the formation of subsurface chimneys. These chimneys provide an environment conducive for gas migration from deeper depths to shallower subsurface. Upon reaching the base of the gas hydrate stability zone, free gas will form gas hydrates. The hydrate formation will arrest upward migration of free gas due to its low permeability, and gas starts accumulating below the BSR to develop over-pressured sediments. If the pressure exceeds the hydrate strength, gas will puncture the hydrate formation and migrates to the seafloor. Gas escape will form pockmarks on the seafloor and create a cold-seep environment (Fig.

3b). One such pockmark shows shallow gas hydrate and associated chemosynthetic communities as shown in Figure 7 (modified after Mazumdar et al., 2021).

5.4. Genesis of gas in the Mannar basin

The Gulf of Mannar is a highly productive basin, and a massive load of organic-rich sediments is deposited on the seafloor throughout the year. The unique physiography favors high biomass in the Gulf of Mannar compared to the neighboring southwest and southeast coast of India (Madhupratap et al., 1992, 1990). Oceanic currents during the Northeast monsoon and obstruction from Ramsethu enhance phytoplankton biomass in the Mannar basin (Jagadeesan et al., 2013). The region has high bio-productivity due to controlled mixing of low saline water from the Bay of Bengal and upwelling water from the Arabian Sea (Koné et al., 2009; Lévy et al., 2007; Tiwari et al., 2006), which plays a crucial role in the nutrient distribution and chlorophyll concentrations. In addition, seasonal pattern of the Indian Ocean Dipole (IOD) also plays a prominent role in supporting high productivity in this region (Sarma, 2006; Thushara and Vinayachandran, 2020). Three small rivers Tamiraparani, Vembar, and Vaipar dump minor amount of sediments in the Gulf of Mannar (Rao et al., 2008). Due to its unique physiography with the restrictive movement of oceanic currents, the organic matter produced in the Gulf of Mannar is restricted to the basin. The organic matter decomposes into hydrocarbon gases at greater depth when it encounters high pressure and temperature conditions (Claypool and Kaplan, 1974). The basin lacks extensive faults/ fracture system; therefore, free gas accumulates over time and lead to overpressured sediments. A conceptual model highlighting different factors for gas hydrate formation and distribution in the Mannar basin is shown in Figure 8.

6. Conclusions

The presence of BSR in MCS data acquired from the Mannar basin indicates the likely presence of gas hydrate deposits. The velocity model estimated for MCS data sets shows anomalous high-velocities zones above the BSR, which are interpreted as gas hydrate deposits. The zones of low-velocities below the BSR show the presence of free gas-bearing sediments. Interpretation of seismic data and attributes analysis show chimneys that transport gas from a deep-seated reservoir to shallow subsurface. The main result of the study can be summarized as follows:

- 1) Low-velocities sediments at greater depth may represent a deep-seated gas reservoir, which may be overpressured. The over-pressured sediments may create faults/fractures near weak zones and facilitate the formation of subsurface chimneys. Mannar basin is devoid of any large scale subsurface faults/fractures, although small scale subsurface fractures are observed, which are formed due to sediments compaction and fluid expulsions.

- 2) Low-frequency shallow and pull-down structures are frequently observed below the BSR, indicating the widespread presence of deep-seated gas in the Mannar basin. Unique physiography setting and restrictive movement of organic-rich sediments create a favorable environment for the genesis of hydrocarbon gas through the decomposition of organic matter.
- 3) Free gas-bearing zones are observed near the chimneys, indicating chimneys' role in providing pathways conducive for migration of deep-seated gas up to the hydrate stability zone. In exceptional cases, chimneys may extend up to the seafloor, allowing gas migration to the seafloor. Rapid expulsion of gas from the seafloor leads to the formation of pockmarks and associated cold-seep ecosystem.
- 4) Sediment sampling of the pockmark show tubeworm associated with the chemosynthetic community, authigenic carbonates with relict shells of *Calyptogena* sp. and shallow methane hydrate confirming methane venting episodes in the Mannar basin.

7. Acknowledgements

We thank the Director, CSIR-National Institute of Oceanography (NIO), Goa and Deputy Director-General, GSI, Mangalore for supporting a joint collaborating program on gas hydrate exploration in the Mannar basin. We also thank the Vessel Management Cell of GSI for providing the state-of-the-art research vessel *Samudra Ratnakar* to acquire 2D MCS data in the Mannar basin. We thank all the cruise participants (SR-06), especially the senior scientists Shri C. Jaya Prakash, Shri G.V. Satyanarayana, Shri P. Ramachandra Rao, Dr. Lukram Ingocha Meetei, Shri V. Govinda Rao, Shri Manoj Kumar Singh, Shri S.K. Arun, Dr. Karthikeyan M, Shri M. Mashood, Shri B. Gopa Kumar, and Shri Vivek Kumar for their cooperation during seismic data acquisition. We also thank the research vessel management group of CSIR-NIO for providing the state-of-the-art vessel *Sindhu Sadhana* for sediment sampling in the Mannar basin. We thank all the participants of the cruise (SSD-070), especially the senior scientists Drs. A. Mazumdar, A. Peketi, and F. Badesab for their cooperation during the sediment sampling. We also acknowledge the CSIR project MLP1601, which supported the development of software codes for the velocity analysis. We thank K. Sudheesh for providing the slot in the Linux cluster for running the velocity analysis code. We would also like to thank Shri. T. Ramprasad, Dr. Sriram Gullapalli, Aditya Kumar, Adarsh Babu, and Pabitra Singha for their support in the geophysics lab. C.K. Mishra would like to thank the CSIR for providing financial support through an award of SRF fellowship. The work was performed under the MLP1703 and OLP2004 programs of CSIR-NIO and the contribution no. is xxx.

References

- Bastia, R., Radhakrishna, M., 2012. Subsurface geology, depositional history, and petroleum systems along the western offshore basins of India. In *Developments in petroleum science* 59, 269-317.
- Berndt, C., Büinz, S., Mienert, J., 2003. Polygonal fault systems on the mid-Norwegian margin: A long-term source for fluid flow. *Geological Society, London, Special Publications* 216 (1), 283-290.
- Berryman, K., Marden, M., Palmer, A., Wilson, K., Mazengarb, C., Litchfield, N., 2010. The post-glacial downcutting history in the Waihuka tributary of Waipaoa River, Gisborne district: Implications for tectonics and landscape evolution in the Hikurangi subduction margin, New Zealand. *Marine Geology* 270 (1-4), 55-71.
- Biondi, B., Symes, W. W., 2004. Angle-domain common-image gathers for migration velocity analysis by wavefield-continuation imaging. *Geophysics* 69, 1283-1298.
- Boswell, R., Collett, T. S., 2011. Current perspectives on gas hydrate resources. *Energy & environmental science* 4 (4), 1206-1215.
- Brown, H. E., Holbrook, W. S., Hornbach, M. J., Nealon, J., 2006. Slide structure and role of gas hydrate at the northern boundary of the Storegga Slide, offshore Norway. *Marine geology* 229 (3-4), 179-186.
- Carcione, J. M., Tinivella, U., 2000. Bottom-simulating reflectors: Seismic velocities and AVO effects. *Geophysics* 65 (1), 54-67.
- Castagna, J. P., Sun, S., Siegfried, R. W., 2003. Instantaneous spectral analysis: Detection of low-frequency shadows associated with hydrocarbons. *The leading edge* 22 (2), 120-127.
- Castagna, J. P., Swan, H. W., 1997. Principles of AVO crossplotting. *The leading edge* 16 (4), 337-344.
- Chand, S., Minshull, T.A., 2003. Seismic constraints on the effects of gas hydrate on sediment physical properties and fluid flow: a review. *Geofluids* 3 (4), 275-289.
- Narasimha, M., Sahu, J. N., Banerjee, B., Zutshi, P. L., Chandra, K., 1995. Evolution of the Cauvery basin, India from subsidence modelling. *Marine and petroleum geology* 12 (06), 667-675.
- Claypool, G. E., Kaplan, I. R., 1974. The origin and distribution of methane in marine sediments. In *Natural gases in marine sediments*, 99-139.
- Collett, T. S., Boswell, R., Cochran, J. R., Kumar, P., Lall, M., Mazumdar, A., Ramana, M.V., Ramprasad, T., Riedel, M., Sain, K., Sathe, A. V., 2014. Geologic implications of gas hydrates in the offshore of India: Results of the National Gas Hydrate Program Expedition 01. *Marine and petroleum geology* 58, 3-28.
- Coren, F., Volpi, V., Tinivella, U., 2001. Gas hydrate physical properties imaging by multi-attribute analysis—Blake Ridge BSR case history. *Marine geology* 178 (1-4), 197-210.

- Crutchley, G. J., Maslen, G., Pecher, I. A., Mountjoy, J. J., 2016. High-resolution seismic velocity analysis as a tool for exploring gas hydrate systems: An example from New Zealand's southern Hikurangi margin. *Interpretation* 4, SA1-SA12.
- Crutchley, G. J., Pecher, I. A., Gorman, A. R., Henrys, S. A., Greinert, J., 2010. Seismic imaging of gas conduits beneath seafloor seep sites in a shallow marine gas hydrate province, Hikurangi Margin, New Zealand. *Marine geology* 272 (1-4), 114-126.
- Curry, J. R., 1984. Sri Lanka : is it a Mid - Plate Platelet ?. *Journal of the National Aquatic Resources Agency* 31, 30-50.
- Dewangan, P., 2015. Gas Hydrate Deposits in the Cauvery-Mannar Offshore Basin, India, in: AGU Fall Meeting Abstracts., OS23B-1997.
- Dewangan, P., Ramprasad, T., Ramana, M. V., Mazumdar, A., Desa, M., Badesab, F. K., 2010. Seabed morphology and gas venting features in the continental slope region of Krishna-Godavari basin, Bay of Bengal: Implications in gas-hydrate exploration. *Marine and Petroleum Geology* 27 (7), 1628–1641.
- Dewangan, P., Ramprasad, T., 2007. Velocity and AVO analysis for the investigation of gas hydrate along a profile in the western continental margin of India. *Marine Geophysical Researches* 28 (3), 201-211.
- Dillon, W.P., Paull, C. K., 1983. Marine gas hydrates: II. Geophysical evidence, in *Natural Gas Hydrates, Properties, Occurrence and Recovery*, edited by J. L. Cox, 73-90.
- Dix, C. H., 1955. Seismic Velocities From Surface Measurements. *Geophysics* 20, 68-86.
- Gullapalli, S., Dewangan, P., Kumar, A., Dakara, G., Mishra, C. K., 2019. Seismic evidence of free gas migration through the gas hydrate stability zone (GHSZ) and active methane seep in Krishna-Godavari offshore basin. *Marine and petroleum geology* 110, 695-705.
- Ecker, C., Dvorkin, J., Nur, A., 1998. Sediments with gas hydrates: Internal structure from seismic AVO. *Geophysics* 63 (5), 1659-1669.
- Goñi, M.A., Ruttenger, K.C., Eglinton, T.I., 1997. Sources and contribution of terrigenous organic carbon to surface sediments in the Gulf of Mexico. *Nature* 389 (6648), 275-278.
- Grevemeyer, I., Rosenberger, A., Villinger, H., 2000. Natural gas hydrates on the continental slope off Pakistan: constraints from seismic techniques. *Geophysical Journal International* 140 (2), 295-310.
- Hajnal, Z., Sereda, I. T., 1981. Maximum uncertainty of interval velocity estimates. *Geophysics* 46, 1543-1547.
- Hedges, J. I., Hu, F. S., Devol, A. H., Hartnett, H. E., Tsamakis, E., Keil, R. G., 1999. Sedimentary organic matter preservation; a test for selective degradation under oxic conditions. *American Journal of Science* 299 (7-9), 529-555.
- Helgerud, M. B., Dvorkin, J., Nur, A., Sakai, A., Collett, T., 1999. Elastic-wave velocity in marine sediments with gas hydrates: Effective medium modeling. *Geophysical Research Letters* 26 (13), 2021-2024.

- Jagadeesan, L., Jyothibabu, R., Anjusha, A., Mohan, A. P., Madhu, N. V., Muraleedharan, K. R., Sudheesh, K., 2013. Ocean currents structuring the mesozooplankton in the Gulf of Mannar and the Palk Bay, southeast coast of India. *Progress in Oceanography* 110, 27–48.
- Jaiswal, P., Dewangan, P., Ramprasad, T., Zelt, C. A., 2012a. Seismic characterization of hydrates in faulted, fine-grained sediments of Krishna-Godavari basin: Unified imaging. *Journal of Geophysical Research: Solid Earth* 117, B04306.
- Jaiswal, P., Dewangan, P., Ramprasad, T., Zelt, C. A., 2012b. Seismic characterization of hydrates in faulted, fine-grained sediments of Krishna-Godavari Basin: Full waveform inversion. *Journal of Geophysical Research: Solid Earth* 117, B10305.
- Koné, V., Aumont, O., Lévy, M., Resplandy, L., 2009. Physical and biogeochemical controls of the phytoplankton seasonal cycle in the Indian Ocean: A modeling study. *Indian Ocean Biogeochemical Processes and Ecological Variability* 185, 350.
- Kumar, P., Collett, T.S., Boswell, R., Cochran, J. R., Lall, M., Mazumdar, A., Ramana, M. V., Ramprasad, T., Riedel, M., Sain, K., Sathe, A.V., 2014. Geologic implications of gas hydrates in the offshore of India: Krishna–Godavari basin, Mahanadi basin, Andaman Sea, Kerala–Konkan basin. *Marine and Petroleum Geology* 58, 29-98.
- Kumar, P., Collett, T. S., Shukla, K. M., Yadav, U. S., Lall, M. V., Vishwanath, K., 2019. India national gas hydrate program expedition-02: operational and technical summary. *Marine and Petroleum Geology* 108, 3-38.
- Kvenvolden, K. A., 1998. A primer on the geological occurrence of gas hydrate. Geological Society, London, Special Publications 137 (1), 9-30.
- Kvenvolden, K. A., 1993. Gas hydrates-geological perspective and global change. *Reviews of geophysics* 31 (2), 173-187.
- Kvenvolden, K. A., 1988. Methane hydrate - A major reservoir of carbon in the shallow geosphere?. *Chemical geology* 71 (1-3), 41-51.
- Kvenvolden, K. A., McDonald, T. J., 1985. Gas Hydrates of the Middle America Trench-Deep Sea Drilling Project Leg 84. Initial Reports Deep Sea Drilling Project 84, 667-682.
- Lee, M. W., Dillon, W. P., 2001. Amplitude blanking related to the pore-filling of gas hydrate in sediments. *Marine Geophysical Researches* 22 (2), 101–109.
- Lévy, M., Shankar, D., André, J. M., Shenoi, S. S. C., Durand, F., de Boyer Montégut, C., 2007. Basin-wide seasonal evolution of the Indian Ocean's phytoplankton blooms. *Journal of Geophysical Research: Oceans* 112, C12014.
- Li, L., Lei, X., Zhang, X., Sha, Z., 2013. Gas hydrate and associated free gas in the Dongsha Area of northern South China Sea. *Marine and Petroleum Geology* 39, 92–101.
- Madhupratap, M., Haridas, P., Ramaiah, N., Achuthankutty, C. T., 1992. Zooplankton of the southwest coast of India: abundance, composition, temporal and spatial variability in 1987. In: Desai, B. (ed.), *Oceanography of the Indian Ocean*. Oxford and IBH Publishing Co. Ltd., New Delhi, 99–112.

- Madhupratap, M., Nair, S. R. S., Haridas, P., Padmavati, G., 1990. Response of zooplankton to physical changes in the environment: coastal upwelling along the central west coast of India. *Journal of Coastal Research* 6, 413-426.
- Majumdar, U., Cook, A. E., Shedd, W., Frye, M., 2016. The connection between natural gas hydrate and bottom-simulating reflectors. *Geophysical Research Letters* 43 (13), 7044-7051.
- Maslin, M. A., Burns, S. J., 2000. Reconstruction of the Amazon Basin effective moisture availability over the past 14,000 years. *Science* 290 (5500), 2285-2287.
- Mazumdar, A., Dewangan, P., Peketi, A., Badesaab F., Sadique M., Sivan, K., Mathai, J., Uma, C., Mishra, C. K., Ghosh, A., Fernandes, W., Tyagi, A., Paul, T., 2021. First report of *Lamellibrachia* tube worm associated chemosynthetic ecosystem from the Indian Ocean. *Journal of earth system science* (accepted).
- Mazumdar, A., Paropkari, A. L., Borole, D. V., Rao, B. R., Khadge, N. H., Karisiddaiah, S. M., Kocherla, M., João, H. M., 2007. Pore-water sulfate concentration profiles of sediment cores from Krishna-Godavari and Goa basins, India. *Geochemical Journal* 41 (4), 259-269.
- Mazumdar, A., Peketi, A., Joao, H. M., Dewangan, P., Ramprasad, T., 2014. Pore-water chemistry of sediment cores off Mahanadi Basin, Bay of Bengal: Possible link to deep seated methane hydrate deposit. *Marine and petroleum geology* 49, 162-175.
- McDonnell, S. L., Max, M. D., Cherkis, N. Z., Czarnecki, M. F., 2000. Tectono-sedimentary controls on the likelihood of gas hydrate occurrence near Taiwan. *Marine and Petroleum Geology* 17 (8), 929-936.
- Milkov, A. V., Sassen, R., 2003. Preliminary assessment of resources and economic potential of individual gas hydrate accumulations in the Gulf of Mexico continental slope. *Marine and Petroleum Geology* 20 (2), 111-128.
- Milkov, A. V., Sassen, R., 2002. Economic geology of offshore gas hydrate accumulations and provinces. *Marine and Petroleum Geology* 19 (1), 1-11.
- Milkov, A. V., Sassen, R., 2001. Estimate of gas hydrate resource, northwestern Gulf of Mexico continental slope. *Marine Geology* 179 (1-2), 71-83.
- Minshull, T. A., Singh, S. C., Westbrook, G. K., 1994. Seismic velocity structure at a gas hydrate reflector, offshore western Colombia, from full waveform inversion. *Journal of Geophysical Research: Solid Earth* 99 (B3), 4715-4734.
- Mishra, C. K., Dewangan, P., Sriram, G., Kumar, A., Dakara, G., 2020. Spatial distribution of gas hydrate deposits in Krishna-Godavari offshore basin, Bay of Bengal. *Marine and Petroleum Geology* 112, 104037.
- Nelder, J. A., Mead, R., 1965. A simplex method for function minimization. *The computer journal* 7 (4), 308-313.

- Pecher, I. A., Henrys, S. A., Ellis, S., Crutchley, G., Fohrmann, M., Gorman, A., Greinert, J., Chiswell, S. M., Party, T. S., Party, S. S., 2008. Erosion of seafloor ridges at the top of the gas hydrate stability zone, Hikurangi Margin, New Zealand - new insights from research cruises between 2005 and 2007. In Proceedings of the 6th International Conference on Gas Hydrates (ICGH 2008), Vancouver, BC, Canada.
- Pecher, I. A., Minshull, T. A., Singh, S. C., Von Huene, R., 1996. Velocity structure of a bottom simulating reflector offshore Peru: Results from full waveform inversion. *Earth and Planetary Science Letters* 139 (3-4), 459-469.
- Pellenbarg, R.E., Max, M.D., 2000. Introduction, physical properties, and natural occurrences of hydrate. In *Natural Gas Hydrate*, 1-8, Springer, Dordrecht.
- Petersen, C. J., Bünz, S., Hustoft, S., Mienert, J., Klaeschen, D., 2010. High-resolution P-Cable 3D seismic imaging of gas chimney structures in gas hydrated sediments of an Arctic sediment drift. *Marine and Petroleum Geology* 27 (9), 1981-1994.
- Popescu, I., Lericolais, G., Panin, N., De Batist, M., Gillet, H., 2007. Seismic expression of gas and gas hydrates across the western Black Sea. *Geo-Marine Letters* 27 (2-4), 173-183.
- Ramprasad, T., Dewangan, P., Ramana, M. V. V., Mazumdar, A., Karisiddaiah, S. M. M., Ramya, E. R. R., Sriram, G., 2011. Evidence of slumping/sliding in Krishna-Godavari offshore basin due to gas/fluid movements. *Marine and Petroleum Geology* 28 (10), 1806-1816.
- Riedel, M., Collett, T.S., Kumar, P., Sathe, A.V., Cook, A., 2010. Seismic imaging of a fractured gas hydrate system in the Krishna–Godavari Basin offshore India. *Marine and Petroleum Geology* 27 (7), 1476-1493.
- Rao, D. V. S., Rao, K. S., Iyer, C. S. P., Chittibabu, P., 2008. Possible ecological consequences from the Sethu Samudram Canal Project, India. *Marine pollution bulletin* 56 (2), 170-186.
- Rao, M. V., Chidambaram, L., Bharktya, D., Janardhanan, M., 2010. Integrated Analysis of Late Albian to Middle Miocene Sediments in Gulf of Mannar Shallow Waters of the Cauvery Basin , India: A Sequence Stratigraphic Approach. In Proceedings of 8th biennial international conference and exposition on petroleum geophysics, Hyderabad, 1-9.
- Rastogi, A., Deka, B., Budhiraja, I. L., Agarwal, G. C., 1999. Possibility of large deposits of gas hydrates in deeper waters of india. *Marine Georesources and Geotechnology* 17 (1), 49-63.
- Rice, W., 2006. Hydrogen production from methane hydrate with sequestering of carbon dioxide. *International Journal of Hydrogen Energy* 31 (14), 1955-1963.
- Riedel, M., Collett, T. S., Kumar, P., Sathe, A. V., Cook, A., 2010. Seismic imaging of a fractured gas hydrate system in the Krishna-Godavari Basin offshore India. *Marine and Petroleum Geology* 27 (7), 1476-1493.
- Ryu, B. J., Riedel, M., Kim, J. H., Hyndman, R. D., Lee, Y. J., Chung, B. H., Kim, I. S., 2009. Gas hydrates in the western deep-water Ulleung Basin, East Sea of Korea. *Marine and Petroleum Geology* 26 (8), 1483-1498.

- Sadeq, D., Alef, K., Iglauer, S., Lebedev, M., Barifcani, A., 2018. Compressional wave velocity of hydrate-bearing bentheimer sediments with varying pore fillings. *International Journal of Hydrogen Energy* 43 (52), 23193-23200.
- Sarma, V. V. S. S., 2006. The influence of Indian Ocean Dipole (IOD) on biogeochemistry of carbon in the Arabian Sea during 1997-1998. *Journal of earth system science* 115 (4), 433-450.
- Sassen, R., Losh, S. L., Cathles III, L., Roberts, H. H., Whelan, J. K., Milkov, A. V., Sweet, S. T., DeFreitas, D. A., 2001. Massive vein-filling gas hydrate: Relation to ongoing gas migration from the deep subsurface in the Gulf of Mexico. *Marine and Petroleum Geology* 18 (5), 551-560.
- Satyavani, N., Sain, K., Lall, M. and Kumar, B. J. P., 2008. Seismic attribute study for gas hydrates in the Andaman Offshore India. *Marine Geophysical Researches* 29(3), 167-175.
- Sava, P., Biondi, B., 2004. Wave-equation migration velocity analysis. I. Theory. *Geophysical Prospecting* 52 (6), 593-606.
- Sheriff, R. E., 2002. *Encyclopedic dictionary of applied geophysics*. Society of exploration geophysicists.
- Shipley, T. H., Houston, M. H., Buffler, R. T., Shaub, F. J., McMillen, K. J., Ladd, J. W., Worzel, J. L., 1979. Seismic evidence for widespread possible gas hydrate horizons on continental slopes and rises. *AAPG bulletin* 63 (12), 2204-2213.
- Singh, S. C., Minshull, T. A., Spence, G. D., 1993. Velocity structure of a gas hydrate reflector. *Science* 260 (5105), 204-207.
- Sloan, E. D., Koh, C., 2007. *Clathrate hydrates of natural gases*. CRC Press.
- Sriram, G., Dewangan, P., Ramprasad, T., Rama Rao, P., 2013. Anisotropic amplitude variation of the bottom-simulating reflector beneath fracture-filled gas hydrate deposit. *Journal of Geophysical Research: Solid Earth* 118 (5), 2258–2274.
- Stork, C., 1992. Reflection tomography in the postmigrated domain. *Geophysics* 57 (5), 680–692.
- Talukdar, S. S. N., 1982. Geology and Hydrocarbon prospects of east coast basins of India and their relationship to evolution of the bay of Bengal. In *Offshore South East Asia Show*. Society of Petroleum Engineers.
- Taner, M. T., Koehler, F., 1969. Velocity spectra - Digital computer derivation applications of velocity functions. *Geophysics* 34 (6), 859-881.
- Taner, M. T., Koehler, F., Sheriff, R. E., 1979. *Complex Seismic Trace Analysis*. *Geophysics* 44 (6), 1041-1063.
- Thushara, V., Vinayachandran, P. N., 2020. Unprecedented Surface Chlorophyll Blooms in the Southeastern Arabian Sea During an Extreme Negative Indian Ocean Dipole. *Geophysical Research Letters* 47 (13), e2019GL085026.
- Tiwari, M., Ramesh, R., Somayajulu, B. L. K., Jull, A. J. T., Burr, G. S., 2006. Paleomonsoon precipitation deduced from a sediment core from the equatorial Indian Ocean. *Geo-Marine Letters* 26 (1), 23-30.

- Trung, N.N., 2012. The gas hydrate potential in the South China Sea. *J. Pet. Sci. Eng.*, 88, 41-47.
- Toldi, J. L., 1989. Velocity analysis without picking. *Geophysics* 54(2), 191-199.
- Westbrook, G. K., Chand, S., Rossi, G., Long, C., Bünz, S., Camerlenghi, A., Carcione, J. M., Dean, S., Foucher, J. P., Flueh, E., Gei, D., Haacke, R. R., Madrussani, G., Mienert, J., Minshull, T. A., Nouzé, H., Peacock, S., Reston, T. J., Vanneste, M., Zillmer, M., 2008. Estimation of gas hydrate concentration from multi-component seismic data at sites on the continental margins of NW Svalbard and the Storegga region of Norway. *Marine and Petroleum Geology* 25 (8), 744-758.
- Whiticar, M. J., Faber, E., Schoell, M., 1986. Biogenic methane formation in marine and freshwater environments: CO₂ reduction vs. acetate fermentation-isotope evidence. *Geochimica et Cosmochimica Acta* 50(5), 693-709.
- Wu, S., Zhang, G., Huang, Y., Liang, J., Wong, H. K., 2005. Gas hydrate occurrence on the continental slope of the northern South China Sea. *Marine and Petroleum Geology* 22 (3), 403-412.
- Yamamoto, K., Terao, Y., Fujii, T., Ikawa, T., Seki, M., Matsuzawa, M., Kanno, T., 2014. Operational overview of the first offshore production test of methane hydrates in the Eastern Nankai Trough. *Proceedings of Offshore Technology Conference, OTC25243*, Houston, Texas, USA
- Yanqun, Q. I. N., Zhang, G., Zhifeng, J. I., Zhi, L. I., Yiping, W. U., Xinglong, W. A. N. G., Liang, X., 2017. Geological features, hydrocarbon accumulation and deep water potential of East Indian basins. *Petroleum Exploration and Development* 44 (5), 731-744.
- Yilmaz, Ö., 2001. *Seismic data analysis: Processing, inversion, and interpretation of seismic data*. Society of exploration geophysicists.
- Yuan, T., Hyndman, R. D., Spence, G. D., Desmons, B., 1996. Seismic velocity increase and deep-sea gas hydrate concentration above a bottom-simulating reflector on the northern Cascadia continental slope. *Journal of Geophysical Research: Solid Earth*, 101 (B6), 13655-13671.

Figure Caption

Figure 1. Map of the study area in the Gulf of Mannar located in the Arabian Sea at the Southern tip of India.

Figure 2. Bathymetry map of the study area in the Mannar basin. Contours show the depth of seafloor at various locations. Several seismic lines oriented in NNE-SSW and WNW-ESE directions are acquired onboard *RV Samudra Ratnakar* as per the collaborative program between CSIR-NIO and GSI for gas hydrate exploration in the Mannar basin. The bold lines show the seismic profiles used in the present study.

Figure 3. Seismic profiles and their corresponding estimated interval velocity section of different inlines and crosslines. Each section shows three different horizons, namely seafloor, BSR (marked as extrapolated base of the GHSZ), and gas horizon. 3a) shows a seismic profile and its interval velocity profile for crossline NS10. Chimney structure is identified and marked within a vertical rectangle box. The ellipse area shows high amplitude reflectors (HAR) and a corresponding low estimated velocity (LEV) zone. The square box in the seismic section shows the zone of reduced amplitude (ZRA) below the gas horizon. 3b) shows seismic profile and its corresponding interval velocity profile for crossline NS11. Two chimneys are identified and marked within a vertical rectangle box. The ellipse area shows HAR and a corresponding LEV in the interval velocity profile. The area demarcated in the square box shows ZRA below the gas horizon. 3c) shows the seismic section and its corresponding estimated velocity profile for inline EW3. Several pull-down structures are identified in the seismic section, which is characterized as LEV regions. Three prominent pull-down structures are marked as ellipses. Two square boxes below the gas horizon show ZRA below the gas horizon. 3d) shows the seismic section and its corresponding estimated velocity profile for inline EW4. Two different zones of HAR are identified, which are associated with LEV as marked by ellipses.

Figure 4. Semblance plots for CIGs selected from different seismic profiles to check the reliability of the auto-picking algorithm. Velocities picked as local maxima by the algorithm are shown as stars. BSR is highlighted in each plot as a dashed horizontal line. High-velocity anomalies above the BSR indicate gas hydrate, and low-velocity anomalies below the BSR indicate free gas (highlighted as solid bars).

Figure 5. Instantaneous amplitude attribute profiles for different seismic lines. Chimneys are characterized as amplitude blanking zone, while regions of low-velocities correspond to high amplitude horizons. Regions of pull-down structures (Fig. 3c) show high amplitude reflection in the amplitude profile (Fig. 5c) below the BSR, and reduced amplitudes are observed below the gas zone.

Figure 6. Instantaneous frequency attribute profiles for different seismic lines. Regions of low velocities below the BSR show lower frequencies owing to seismic attenuation due to free gas.

Figure 7. Sample recovered from a pockmark in the mannar basin during the cruise SSD-070 (modified after Mazumdar et al., 2021) a) *Lamellibrachia* polychaete tubeworm b) fracture filled gas hydrate deposit marked by arrows and c) recovered sample of gas hydrate.

Figure 8. A conceptual model of the genesis of methane gas and hydrate formation in the Mannar basin. a) Decomposition of organic material under suitable pressure and temperature conditions produce methane and other lower hydrocarbon gases as shown by small ellipses. Initial development of faults or fractures due to sediment compaction and release of pore fluids. b) The continuous formation of gases increases the pore pressure and may facilitate multiple fractures in weak zones. c) Combination of multiple fractures into one chimney-like structure facilitates migration of hydrocarbon gases from deep-seated gas reservoirs. As gases reach the gas hydrate stability zone, they form gas hydrate and develop BSR. In exceptional cases, the chimney may extend to the seafloor, leading to methane seeps with a cold-seep ecosystem.

Figure 1

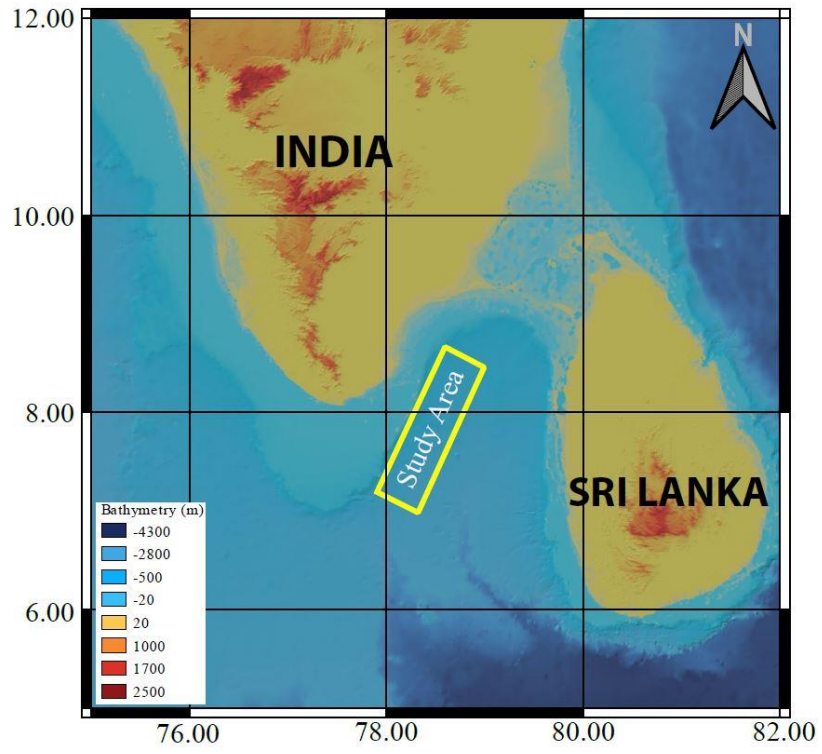


Figure 2

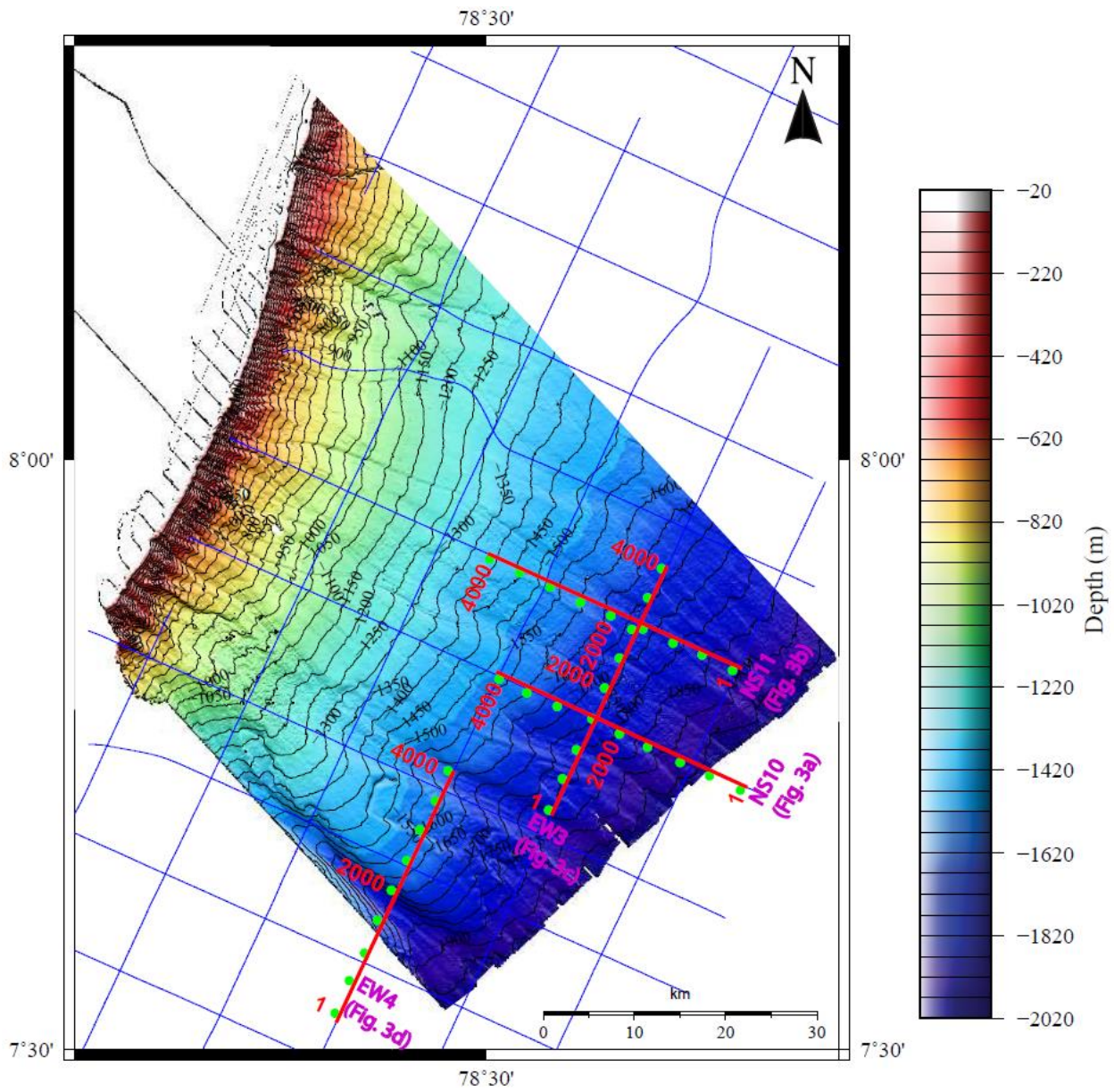


Figure 3

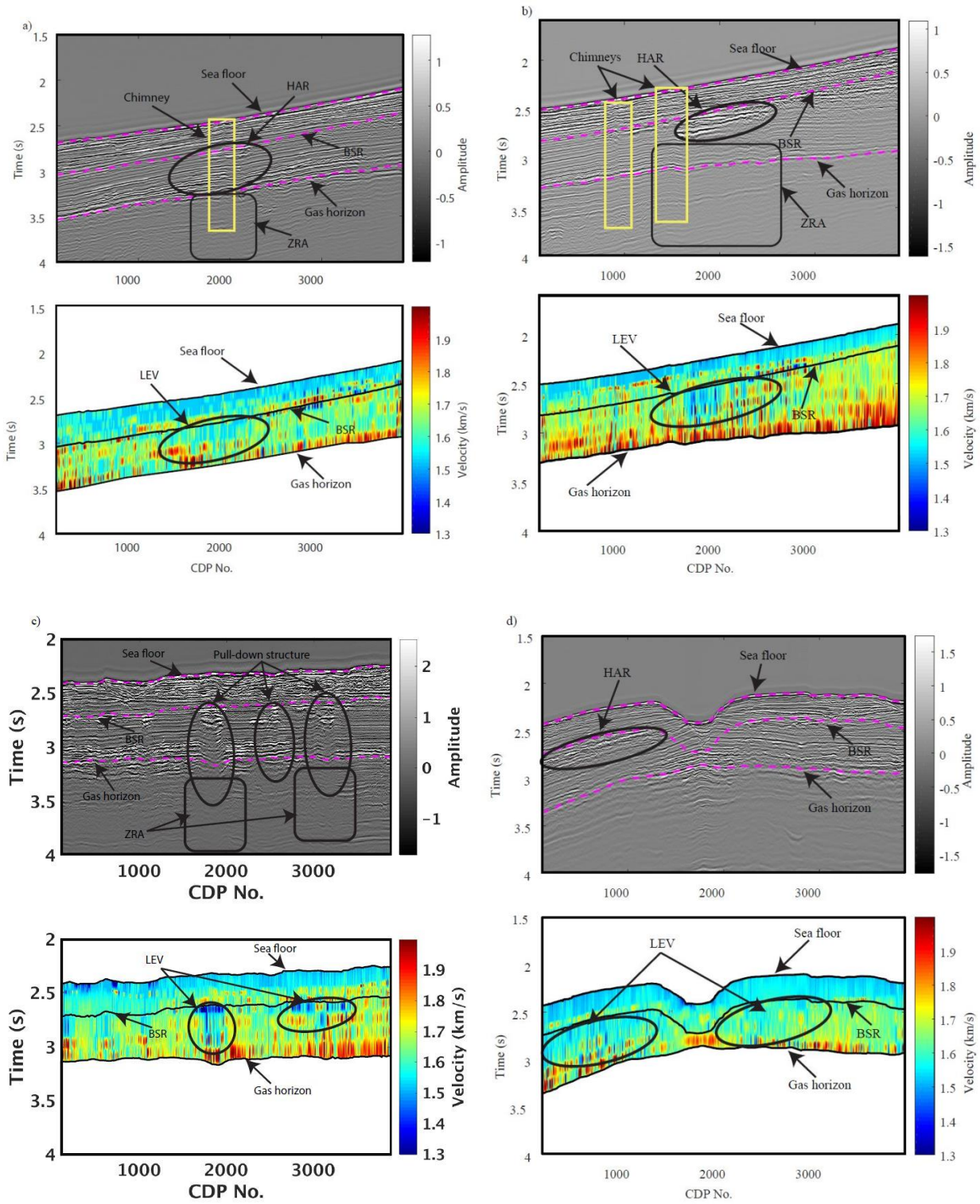


Figure 4

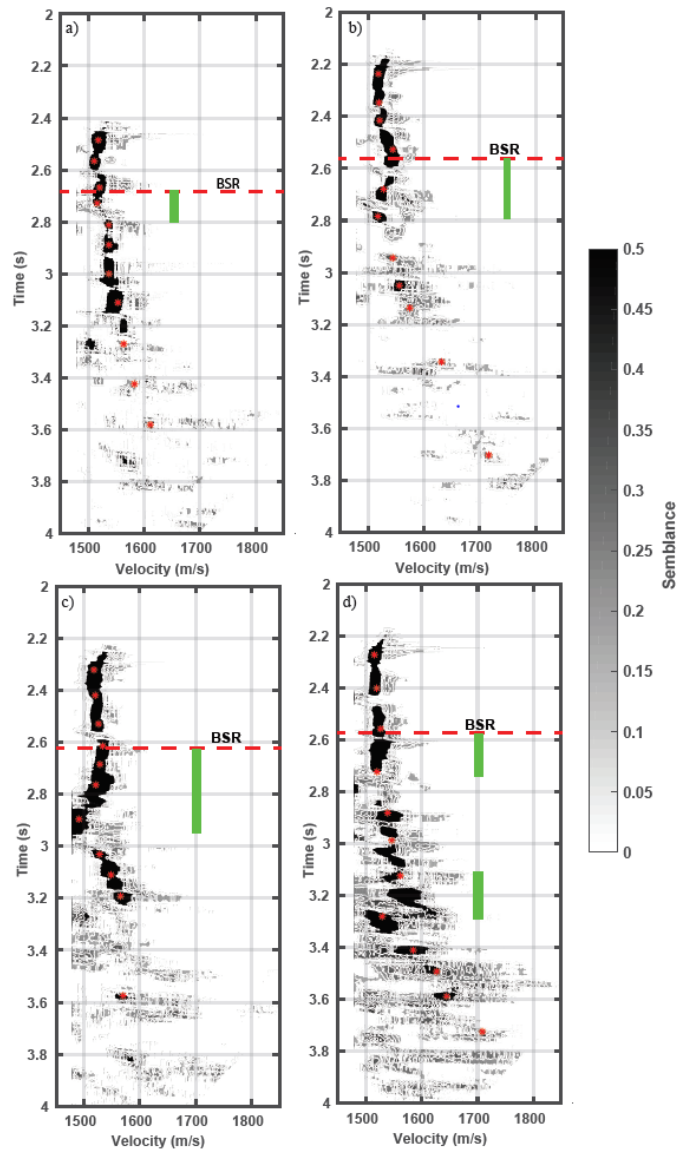


Figure 5

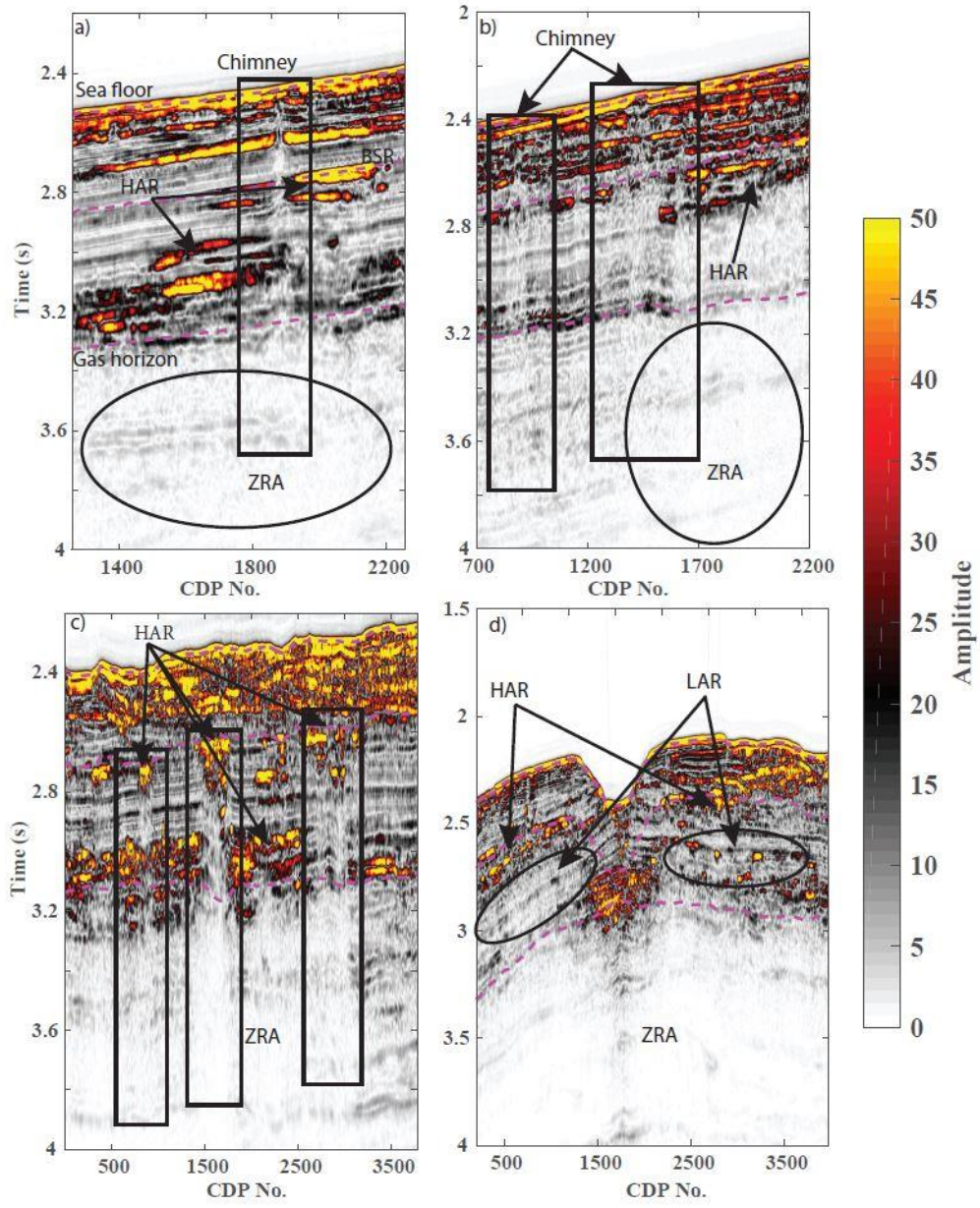


Figure 6

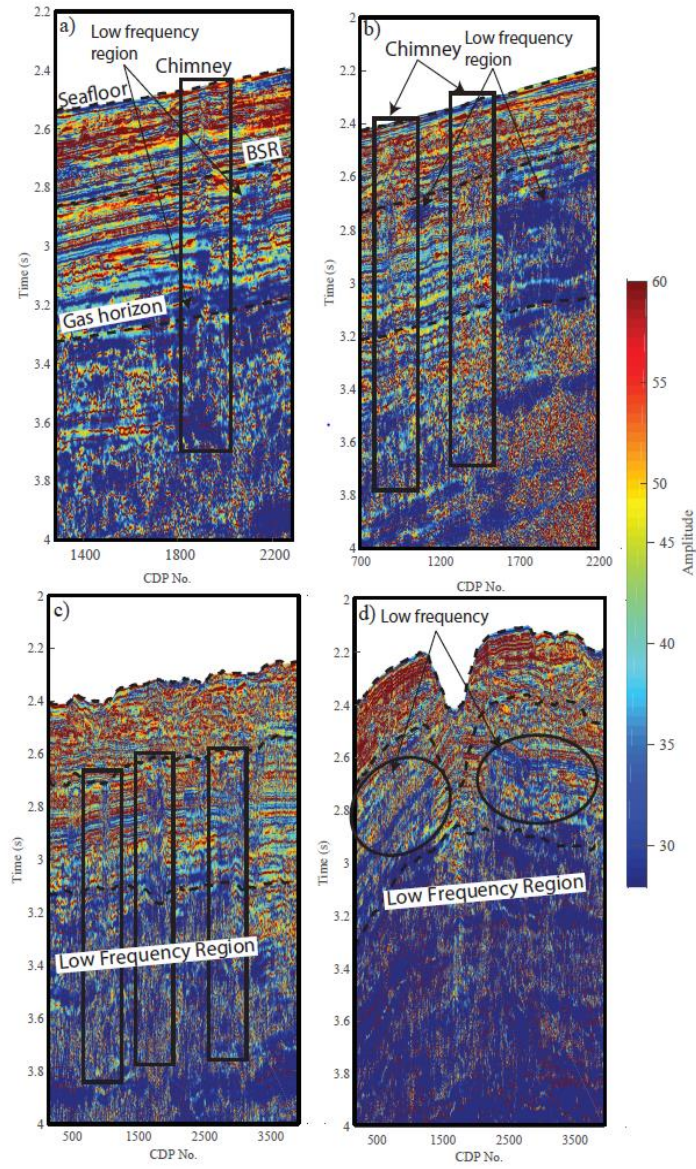


Figure 7

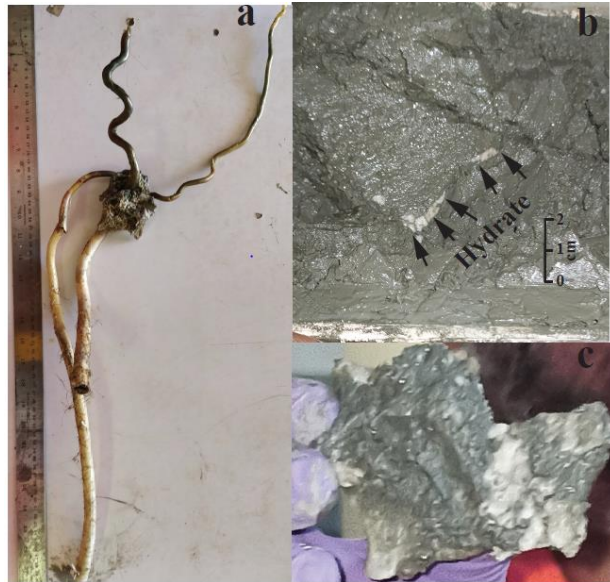


Figure 8

